⟨Invited Review Article⟩

Sizing of Spray Particles Using Image Processing Technique

Sang Yong Lee*, **Yu Dong Kim**

Department of Mechanical Engineering, Korea Advanced Institute of Science and Technology,
Science Town, Daejeon 305-701, Korea

The image processing technique is simple and, in principle, can handle particles with various shapes since it is based on direct visualization. Moreover, a wide measurement area can be covered with appropriate optical arrangement. In the present paper, various techniques of image processing for sizing and counting particles are reviewed and recent developments are introduced. Two major subjects are discussed in detail : identification of particles (i.e., boundary detection and pattern recognition) and determination of in-focus criteria. Finally, an overall procedure for image processing of spray particles is suggested.

Key Words : Image Processing, Particle Size Measurement, Spray

1. Introduction

Various optical techniques have been being used as the non-intrusive method to size drops and particles, such as the phase-Doppler particle analysis (PDPA), light scattering method and the image processing technique (Chigier, 1983).

The PDPA technique is based on processing of Doppler effect of the Mie scattering signals coming from the particles passing through a measuring volume. Thereby, simultaneous measurement of size and velocity of individual particles is available. Though the fiber optics are adopted in the system, however, the optical alignment is still cumbersome and the price of the equipment is rather expensive. Other technique widely being used is the light scattering method based on the Fraunhofer diffraction theory (Swithenbank et al., 1977). This technique is relatively simple and also has an advantage of easy alignment. However, this has disadvantages

of multiple scattering and vignetting effects (Wild and Swithenbank, 1986) that have to be corrected empirically.

The above two techniques are deducing the particle size information from the optical signals scattered from individual or group of particles in the measuring volume assuming that the particles are all spheres. Thus, basically, only the spherical particles should be processed with those techniques for accurate measurement (Malot and Blaisot, 2000). On the other hand, in principle, various non-spherical particles can be processed through the image processing technique because it is based on direct visualization, and wide application is possible. Moreover, the measurement accuracy of the image processing techniques is relatively insensitive to the optical properties of the particles compared to the other techniques, and the optical alignment is much easier (Lecuona et al., 2000). However, the image processing technique also has shortcomings : a number of image frames have to be processed to get the statistically meaningful distributions for a control volume because the data acquisition rate is usually low (i.e., number of spray particles contained in an image frame is usually small) (Nishino et al., 2000). Also, the accuracy of the results strongly depends on the depth of field

---

* Corresponding Author,
  E-mail : sangyonglee@kaist.ac.kr
  TEL : +82-42-869-3026; **FAX** : +82-42-869-8207
  Department of Mechanical Engineering, Korea Advanced Institute of Science and Technology, Science Town, Daejeon 305-701, Korea. (Manuscript **Received** February 3, 2004; **Revised** April 21, 2004)

criterion (Chigier, 1991 ; Nishino et al., 2000).

The ultimate goal of the image processing research is to identify the objects of interest (spray particles in the present case) and to measure their sizes. The in-focus criteria should be provided to decide whether to count or not, and the boundaries of objects should be detected and identified effectively. The particle identification process includes determination of the threshold level for boundary detection, separation of primary particles from their agglomerated or overlapped images, and treatment of non-spherical particles. Finally, once the particles are identified, those are sized and counted to give the size distribution.

In the present paper, various image-processing techniques are discussed and compared to each other to find out their merits and demerits in detail ; and then recent developments to improve the measurement accuracy and efficiency of these techniques are briefly introduced.

2. Fundamental System Hardware

Basically, the system hardware for image processing consists of a light source, a camera and a computer with the accessories as shown in Fig. 1. In most cases, the camera, object and the light source are placed in line with backward illumination. However, for image processing of fluorescent particles, the technique of side illumination with a laser sheet is often used. An instantaneous light source (flash strobolight) is used to capture the frozen images of spray particles in
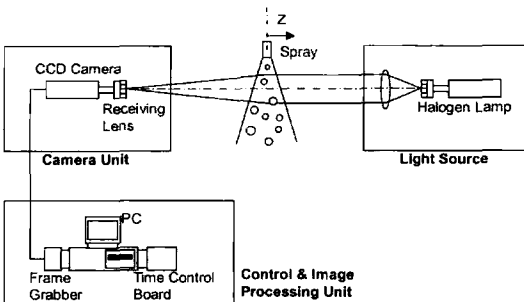
Fig. 1 Hardware setup of image processing technique (Kim, 2000)

the flow field. Thus the flashing duration should be as short as possible to capture small or high-speed particles. For the camera system, traditional film cameras may be used ; however CCD (Charge-Coupled Device) cameras are widely being adopted to eliminate the manual scanning process for digitization. Computers are equipped with a time control board and a frame grabber to synchronize signals and to store the captured images. The computer also processes the stored images to get the final results.

3. In-Focus Criterion

The depth-of-field effect is one of the major factors influencing the measurement accuracy. There are two possible error sources concerned with the depth-of-field effect (Chigier, 1991 ; Nishino et al., 2000). One is the ambiguity in defining the boundaries of the particles that are placed outside the focal plane. The ambiguity increases as the particles are located farther from the focal plane. Thus, one should judge whether to count or not from the degree of ambiguity. This has been studied in some detail by Kim and Kim (1994) and will be discussed later. Another is the dependency of the depth of field on the particle size. As the particle size becomes smaller, the depth of field drastically decreases, and hence, small particles in a pre-determined measuring volume are more likely to be missed in counting. As a result, the particle size distribution is biased toward a larger size region (Oberdier, 1984 ; Koh et al., 2001). Therefore there should be a way to correct this effect by adjusting the depth of field corresponding to the particle size, which will also be introduced later.

As an indicator of the in-focus criteria, either of the following concepts may be adopted : the gray-level gradient at the particle boundaries (Fantini et al., 1990 ; Lecuona et al., 2000) or the contrast value between the particles and the background of the image frame (Kim and Kim, 1994 ; Lebrun et al., 1996 ; Malot and Blaisot, 2000). Later, Koh et al.(2001) proposed appropriate size ranges for each concept.

3.1 Criterion by gray-level gradient

As a particle is located farther from the focal plane, the gray level at the edge of the particle image changes more gradually as shown in Fig. 2 (Koh et al., 2001), and the gray-level gradient can be used to express the degree of focus of the particles (Ramshaw, 1968 ; Fantini et al., 1990). In this figure, z denotes the axial distance from the focal plane with the positive value being the direction toward the CCD camera as shown in Fig. 1. Figure 3 illustrates typical gray-level profiles for an in-focus and an out-of-focus particle (Fantini et al., 1990). The gray-level gradient of the focused particle is steeper than that of the unfocused one. Two gray levels, I_2 and I_3, defining a "halo" around the particle can be identified, which correspond to diameters d_2 and d_3, respectively. Then the width of the halo $(\Delta d/2)$ equivalent to $(d_3-d_2)/2$ can be used as an index of in-focus criteria (Fantini et al., 1990). That is, if $\Delta d/2$ is larger than $H(d)$, a function of

the particle diameter obtained through the calibration process, the corresponding particle is eliminated in counting. Figure 4 exhibits the calibration results for various particle diameters ranging from 30 microns to 340 microns. Thus, by using the calibration result with the halo width, actual particle diameters could be predicted from the measured values.

Lecuona et al. (2000) also employed the concept of gray-level gradient to eliminate the unfocused particles in simultaneous measurement of particle sizes and velocities. There, they defined the in-focus parameter as

$$inf = K \frac{grad_{max}}{grad_{comp}} \tag{1}$$

with the following definition :

$$grad_{comp} = \frac{I_{max} - I_{back}}{d_p} \tag{2}$$

Here, $K = 0.01$ and d_p represents the particle diameter. Also, I_{max} and I_{back} are the maximum and background gray levels, respectively. The gray level gradient at the edge of the particles, $grad_{max}$, is obtained from the Sobel operators (Gonzalez and Woods, 1993). This parameter is insensitive to the local brightness of the image frame. Figure 5 shows variations of inf with the distance from the focal plane for different aperture numbers (F) and particle (glass sphere) diameters ranging between 0.5 mm and 3 mm.
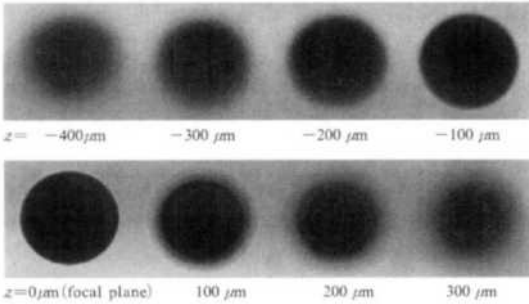
Fig. 2 Change of particle images with distance from the focal plane (300-micron particle)
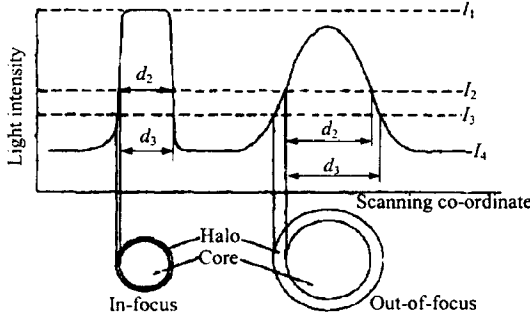
Fig. 3 Drop image intensity profiles (Fantini et al., 1990)
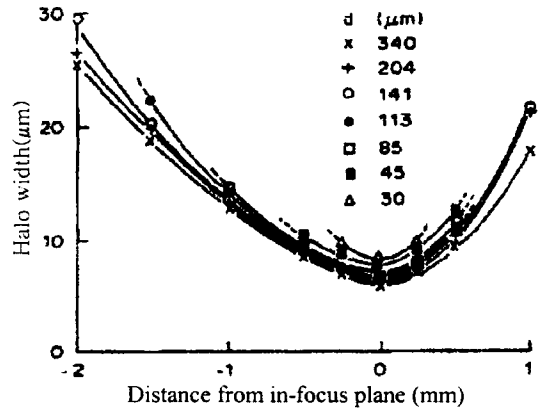
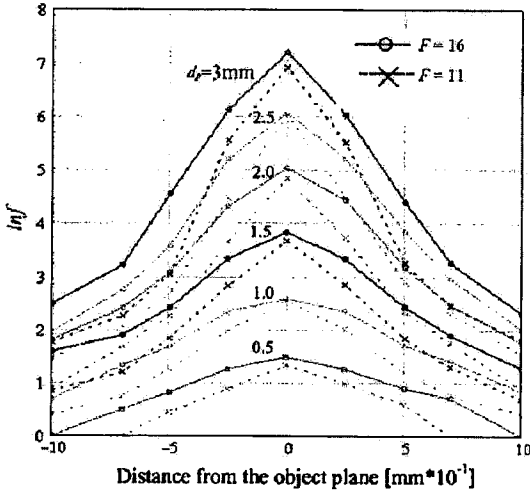**Fig. 4** Halo width variation with position in field (Fantini et al., 1990)

Fig. 5 Variation of *inf* with respect to axial distance from object plane (Lecuona et al., 2000)

Based on this calibration curve, critical value of *inf* for each size can be determined by imposing a proper value of the depth of field, and the particles with smaller *inf* are considered as out of focus.

3.2 Criterion by value of contrast

Kim and Kim (1994) performed an extensive study on the image processing technique to size liquid drops less than 30 microns discharged from a fuel injector. Their study includes the determination of the threshold gray level and in-focus criterion. They introduced the concept of the normalized value of contrast (*VC*) to determine if the drops are in focus or not. With this concept, the depth-of-field correction has been performed for each size of drops. This criterion is known to be effective for sizing small drops, and will be discussed later along with the work by Koh et al.(2001).

In the work of Lebrun et al.(1996), out-of-focus images are deconvoluted with the assumption of a Gaussian point-spread function, where the spatial parameters increases with the distance from the focal plane. Similar approach has been performed independently by Malot and Blaisot (2000). The intensity (gray level) distribution on CCD plane may be expressed with the following

convolution :

$$I(r) = A(r) * h(r) \qquad (3)$$

where $A(r) = 1 - \text{circ}(r/d)$ and d is the geometric image radius. The value of $\text{circ}(r/d)$ is unity for $r \leq d$ and zero elsewhere. Also

$$h(r) = \frac{8}{\pi \sigma^2} \exp\left(\frac{-8r^2}{\sigma^2}\right) \qquad (4)$$

which is the Gaussian point spread function (PSF) and σ represents the spatial parameter of PSF. The value of σ increases as the distance from the focal plane increases. The image contrast is defined as

$$C = \frac{I(\infty) - I(0)}{I(\infty) + I(0)} \qquad (5)$$

where $I(\infty)$ and $I(0)$ are the intensities at $r \rightarrow \infty$ and at the image center, respectively. The image contrast can be expressed in terms of particle diameter (d) and the degree of out-of-focus (σ). In their case, the gray-level threshold was set to $I = 0.55\{I(\infty) - I(0)\} + I(0)$. Thereby, through the calibration process with the particles of known sizes, a relationship between the true value and the measured one could be obtained. According to Lebrun et al.(1996) and Malot and Blaisot (2000), the dependency of the ratio between the measured and true radii on the image contrast (C) becomes weaker as the value of C approaches unity. This implies that this criterion is not effective to judge the degree of focus for large particles.

3.3 Unified in-focus criterion

From the previous discussions, it can be realized that the criterion of gray-level gradient is mostly suitable to large particles whereas the criterion of contrast value is for small particles. In this view, Koh et al.(2001) suggested to adopt both criteria by introducing the appropriate particle-size ranges for each case. For the particles smaller than 30 microns, based on their optical arrangement, the normalized value of contrast (Kim and Kim, 1994) defined as

$$VC = \frac{G_{LB} - G_{OM}}{G_{LB}} \qquad (6)$$

was used as an index of the in-focus criterion. Here, G_{LB} and G_{OM} represent the local background and the object minimum gray levels, respectively, as shown in Fig. 6. Figure 7 shows the variation of VC with the distance from the focal plane for particle size range of 8-300 microns. The VC value becomes the largest at or near the focal plane and decreases as becomes unfocused. However, the variation appears gradual with the larger particles. This implies that VC is no longer effective as the index of the degree of focus. In other words, for a large out-of-focus particle, the radius $(d/2)$ is always greater than the boundary width (w), and the value of G_{OM} remains unchanged.

For particles larger than 30 microns, the concept of the gradient indicator (GI) was introduced as an index of the in-focus criterion, defined as
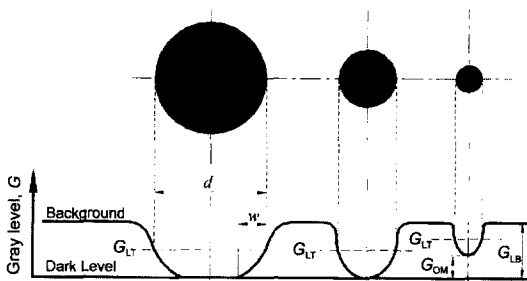

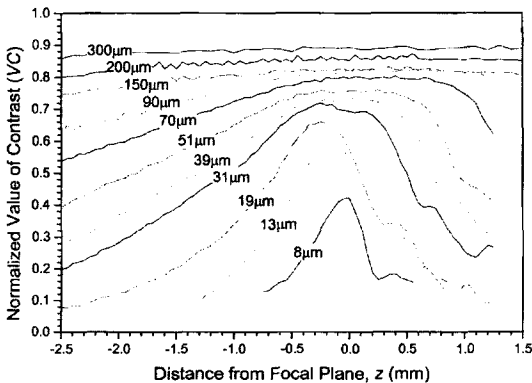**Fig. 6** Gray level changes with different particle size (Koh et al., 2001)

$$GI = \frac{|\nabla G|}{\left[\dfrac{G_{max} - G_{min}}{2\Delta x}\right]} \qquad (7)$$

which has the similar concept with inf (Eq. (1)) of Lecuona et al. (2000). Here, from Fig. 8, the gray level gradient is

$$|\nabla G(x, y)| = \left[\left(\frac{\partial G}{\partial x}\right)^2 + \left(\frac{\partial G}{\partial y}\right)^2\right]^{\frac{1}{2}} \qquad (8)$$

and, for pixel #5, the gray level gradients in x and y directions can be expressed with the Sobel operators as follows;

$$\frac{\partial G}{\partial x} = \frac{(G_3 + 2G_6 + G_9) - (G_1 + 2G_4 + G_7)}{8\Delta x}$$

$$\frac{\partial G}{\partial y} = \frac{(G_7 + 2G_8 + G_9) - (G_1 + 2G_2 + G_3)}{8\Delta y} \qquad (9)$$

As shown in Fig. 9, the values of GI show the maximums at or near the focal plane and decrease as away from the focal plane. Thus GI can be used as an index of the degree of focus as well. Figure 10 shows the depth of field variation with
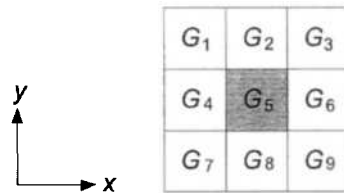

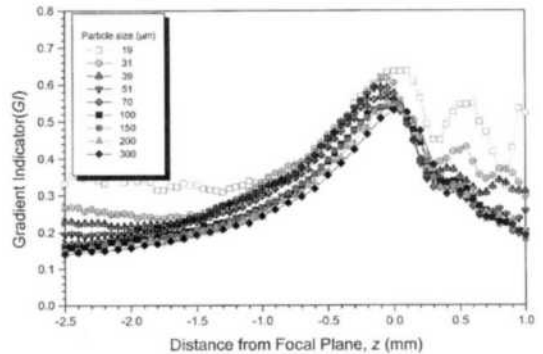**Fig. 8** Numbering of the pixels to express gray level gradient at pixel #5

Fig. 7 Variation of normalized value of contrast (VC) with distance from focal plane for each particle size (Koh et al., 2001)
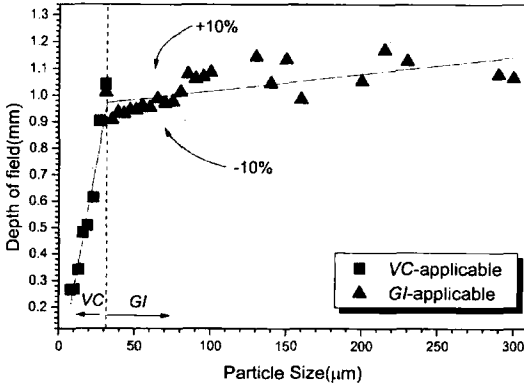

Fig. 9 Variation of gradient indicator (GI) with distance from focal plane for each particle size (Koh et al., 2001)

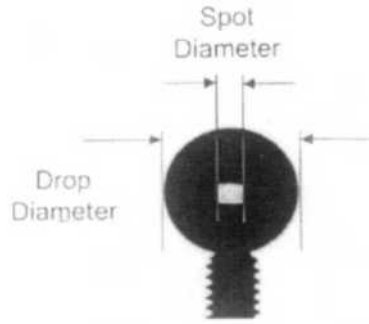Fig. 10 Variation of depth of field with particle size (Koh et al., 2001)

Fig. 11 Sample Image of Glass Sphere (Saylor and Jones, 2002)

the particle size ranging from 10 to 300 microns, mostly covers the fuel spray drops. Here, by introducing two different indices, *VC* and *GI*, the measurement accuracy could be maintained below ten percent. The relationship between the depth of field and the particle size is very useful because it can be utilized in the process of the depth-of-field correction for a fixed measuring volume (Kim and Kim, 1994).

3.4 Other related works

The previous methods introduced in the earlier sections are the techniques generally used to resolve the out-of-focus problem. However, there are some other works related to determination of the in-focus criteria (Nishino et al., 2000 ; Saylor and Jones, 2002).

Saylor and Jones (2002) developed an image-processing algorithm to improve the performance of the rain imaging system (RIS) for raindrop size measurement. In order to secure a sufficient number of drops in a single image frame, the depth of field should be increased. At the same time, increasing of the depth of field causes the increase of the measurement error since the sizes of the unfocused particles appears to be different from the true values. Therefore, in their work, a method to increase the depth of field was proposed without losing the measurement accuracy. With the backward illumination, a bright spot is observed at the center portion of the transparent particles as shown in Fig. 11. The bright

spot is the image of the light source, as seen through the drop, and appears sharp when the drop is at the focal plane. (The light source used in their experiment has a rectangular shape.) As the drop is away from the focal plane, the spot becomes ambiguous. Saylor and Jones (2002) showed that, by using glass spheres, parameter α defined as the ratio between the spot diameter and the drop diameter (Fig. 11) depends solely on the distance from the focal plane. However, the sizes of the glass spheres tested were ranging from 4 mm to 10 mm and only applicable to large transparent particles such as raindrops. Lecuona et al. (2000) also have noted that the sharpness of the image may be used as an indicator of degree of focus.

Nishino et al. (2000) used two CCD cameras to obtain stereo images of particles for simultaneous measurement of size and three velocity components of particles in dispersed two-phase flow. The technique developed was capable of sizing 10-500 microns. As a part of their experiment, the resolution of the depth-of-field effect in particle sizing was considered. They noted that the diameters of small particles (smaller than 40 microns) tend to be overestimated while those of the larger ones (larger than 100 micros) show the opposite trend.

4. Particle Identification

The shape and size information of the particles in an image frame is obtained through the particle identification process. The general proce-

dure is to separate out the particles from the background of the image frame by using the boundary detection algorithms, and then the size and shape of the binary images of the particles are measured and recognized by using the pattern recognition algorithms. The particle diameter can be deduced once the number of pixels occupied by the particle image and the scale factor (length/pixel) of the optical system are given. The details are discussed in the following sections.

4.1 Boundary detection

There are two indicators mainly used to detect the particle boundaries : gray-level threshold and gray-level gradient.

Gray-level threshold is the indicator most widely considered in detecting the particle boundaries since it is simple to use (Otsu, 1979 ; Fantini et al., 1990 ; Lee et al., 1991 ; Kim and Kim, 1994 ; Lebrun et al., 1996 ; Kim et al., 1999 ; Kim, 2000 ; Malot and Blaisot, 2000 ; Sudheer and Panda, 2000 ; Koh et al., 2001 ; Saylor and Jones, 2002). For a given image frame, the portions with the gray level lower than a threshold value are counted as particles and the rest parts are considered as the background. In this case, the number of the detected particles as well as their sizes depends on the threshold level, and care should be taken to decide this value. There are two different ways to determine the threshold gray level ; taking an appropriate value simply between the gray levels of each particle and the background (Kim and Kim, 1994 ; Lebrun et al., 1996 ; Kim et al., 1999 ; Kim, 2000 ; Malot and Blaisot, 2000 ; Koh et al., 2001), or obtaining from the gray-level histogram of the image frames (Otsu, 1979 ; Fantini et al., 1990 ; Lee et al., 1991 ; Kim, 2000 ; Sudheer and Panda, 2000 ; Saylor and Jones, 2002).

As a simple thresholding criterion, Kim and Kim (1994), Kim et al.(1999) and Koh et al. (2001) have taken the threshold value (T), defined as (Fig. 6)

$$T = \frac{G_{LT} - G_{LB}}{G_{OM} - G_{LB}} \qquad (10)$$
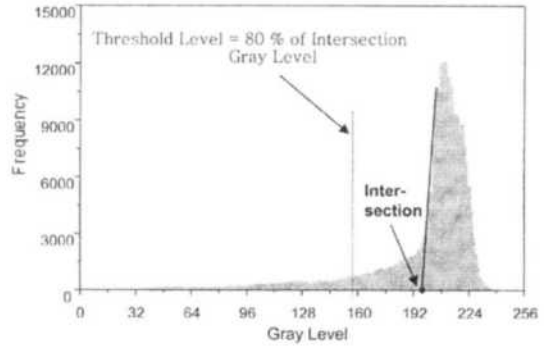
Fig. 12 Typical histogram of a spray image and determination of threshold level (Kim, 2000)

to be 0.5. However, the value strongly depends on the quality of the image frames and Lebrun et al. (1996) and Malot and Blaisot (2000) suggested $1-T$ to be 0.55 and 0.61, respectively, through their own calibration process.
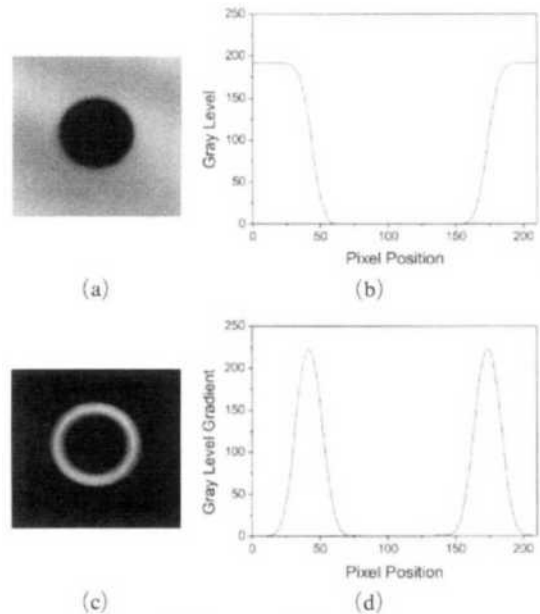
The method using the gray-level histogram has been adopted in the works of Otsu (1979), Lee et al.(1991), Kim (2000) and Sudheer and Panda (2000). Figure 12 shows a typical gray-level histogram of a spray image, in which the gray-level range near the peak value corresponds to the background. However, the gray levels of the particles are mostly zero and, though not shown in the figure, there is a sharp local peak coincides with the ordinate of this plot. Therefore, Lee et al.(1991) have taken one-half of the gray level corresponding to the peak of the histogram as the threshold value. On the other hand, as the threshold level to identify the particles, Kim (2000) took the 80%-value of the intersection of the abscissa and the tangential line at the steepest gradient of the histogram as illustrated in Fig. 12. More sophisticated approach has been attempted by Otsu (1979) and adopted later by Sudheer and Panda (2000). They determined the threshold value based on the zeroth and the first order cumulative momentums from the gray-level histogram. To help illustrating this method, a schematic of the gray-level histogram was given in Fig. 13 along with the important parameters. Here, let μ_0 and μ_1 represent the mean gray levels (first-order cumu-
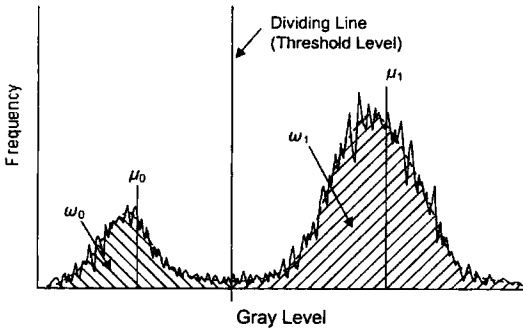
Fig. 13   Illustration of the method of Otsu (1979) for gray-level threshold

Fig. 14   Sample image and its gray level gradient

lative moments) of each gray-level group of the histogram, respectively, divided by a vertical line in the figure. Similarly, let ω_0 and ω_1 be the numbers of the pixels belong to each gray-level group (i.e., the zeroth-order cumulative moments). Then the line dividing the gray-level group in Fig. 13 would represent the optimal threshold if the value of $\omega_0\omega_1(\mu_0-\mu_1)^2$ is the maximum. It has an advantage of avoiding consideration of the local valleys of the histogram by using the integrated values. However, it should be mentioned that the threshold level determined by this method varies with the change of the number concentration of the particles contained in an image frame even though the size distribution remains the same.

Gray-level gradient method is based on the assumption that the gray-level variation is the steepest at the particle boundaries as illustrated in Fig. 14. Figure 14(a) is the original image of a particle, while Fig. 14(c) is its converted image in the plane of the gray-level gradient. Figs. 14 (b) and (d) are the plots of the gray level and its gradient corresponding to Figs. 14(a) and (c), respectively. The brightest part of the ring-shaped image in Fig. 14(c) corresponds to the steepest gradient of the gray level. Kim and Lee (2002) used this method in identifying the primary particles from the images of heavily overlapped particles. From the plot of gray-level gradient, as exemplified by Fig. 14(d), an appropriate threshold value was imposed to recognize the particle boundary. Here, there may be more than one pixel having the gradient greater than this threshold

value; and they went through the boundary thinning process down to the 1-pixel thickness. On the other hand, Nishino et al.(2000) traced the maximum gradient points along the edge of the particle boundary by curve fitting.

4.2 Pattern recognition and size measurement

Once the particle boundaries are sought and the binary images are obtained, the shape and size of the particles can be identified and measured. The shapes of the particles are either spherical (circular) or non-spherical (non-circular). Besides, the separation of the overlapped particles is performed in this stage.

The common method to measure the particle size is finding of the equivalent diameter of a circle having the same projected area regardless of its original shape (Fantini et al., 1990 ; Lebrun et al., 1996 ; Sudheer and Panda, 2000). For spherical particles, the radius can be obtained from the mean distance from the boundary pixels to the mass center as follows :

$$Radius = \frac{1}{N}\sum_{k=1}^{N}\sqrt{(x_k-x_c)^2+(y_k-y_c)^2} \quad (11)$$

$$Center(x_c, y_c) = \left(\frac{1}{N}\sum_{k=1}^{N}x_k, \frac{1}{N}\sum_{k=1}^{N}y_k\right) \quad (12)$$

Here, N, x_k and y_k denote the number of pixels at the image boundary and their x-y locations in the plane, respectively. The result is mostly acceptable because the particles are spherical or nearly spherical. However, it gives inaccurate results for the partly detected or overlapped images of particles. To overcome this difficulty, Kim et al.(1999) proposed to find the circumcenter of the particle image instead of the mass center. Figure 15 illustrates the concept of this method. Once points A, B, and C are selected from the boundary pixels, a triangle ABC is determined as in Fig. 15(a). Then the circumcenter (point O) of this triangle is found at the cross point of the perpendicular lines (OP, OQ and OR) bisecting each side. When there are more than three data points at the particle boundary, a circle that best fits those points should be found. That is, with N data points, $N(N-1)(N-2)/6$ triangles and their circumcenters are found, and from the arithmetic mean values of the center locations and the radii of the circles, a circle that best fits all data points can be determined. Here, it should be noted that the three data points should be distant from each other to avoid an erroneous result as illustrated by adjacent points D, E and F in Fig. 15(a), and the details on this technique are explained in the work of Kim et al.(1999). The circumcenter-based concept has the advantage when only the partial data points are available for analysis as

shown in Fig. 15(b).

An image processing method based on the correlation analysis in the frequency (Fourier) domain has been reported by Cruvinel et al. (1999). First, reference (standard) images of a particle with various sizes are prepared. Then the particles in the image frames of interest were sought by matching their patterns with the reference images using the Fourier transform process. Figure 16 illustrates this technique in detail. Figure 16(a) shows an input image treated with a threshold area processing. Figure 16(b) shows the standard image of a particle to be recognized from the input image. Figures 16(c) and (d) are the Fourier spectra of the input image and the standard image. Figure 16(e) is the correlation map of the spectra obtained through convolution, where the particle of interest shows the highest correlation (i.e., the brightest spot appears), and Fig. 16(f) is the final result recognizing the particle image having the same radius with the standard image.

For overlapped particle images, Kim and Lee (1990), Lecuona et al.(2000) and Malot and Blaisot (2000) simply eliminated them since they are considered either odd-shaped foreign materials or erroneously detected. This concept is acceptable only when the drop area fraction (DAF) of the image frame is low since the chances of the particle overlap are usually small. Zhang and Ishii (1995) and Shen et al.(2001) reported their works on the treatment of the overlapped particles, but the details are not given
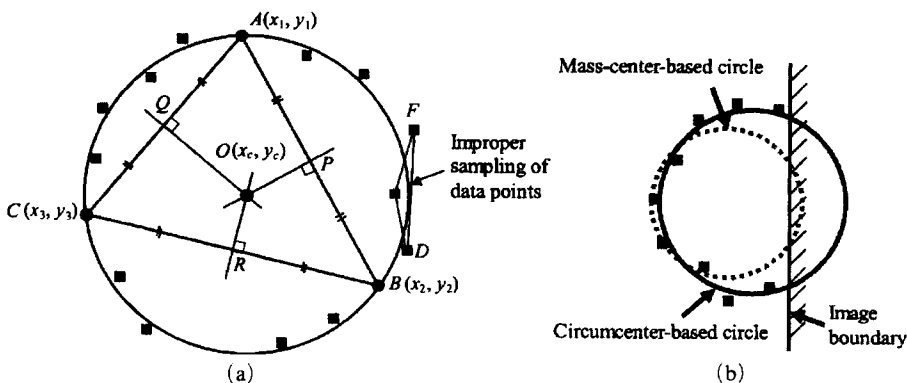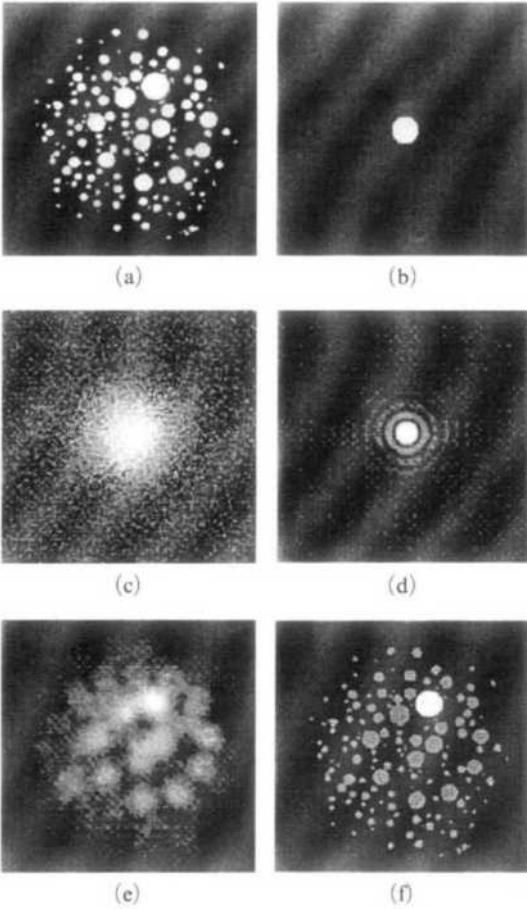

Fig. 15 Detection of the circumcenter (Kim et al., 1999)

Fig. 16 Result of drop identification (Cruvinel et al., 1999)

in their paper. Thus, in the present review, the methods of the particle separation using the Hough transform (Kruis et al., 1994 ; Crida and de Jager, 1997 ; Kim and Lee, 2002), the boundary curvature detection (Kim et al., 2001), and the convex-hull method (Kim et al., 1999) are discussed.

Using of the Hough transform is very effective way to handle the heavily overlapped particles. Basically, the primary particles are separated out from the agglomerated image, and at the same time, each particle size can be estimated. Figure 17 illustrates the principle of the Hough transform process to identify a circle image. The rectangular symbols in Fig. 17(a) (except for pixels a, e and f) are the boundary pixels of a particle to be identified. Circle A is the true circle with radius R and the center is located at $a(X, Y)$. With the assumed radius (R) of circle A, its center should exist somewhere at distance R from the boundary pixels. For example, the center of circle A should be a peripheral point of circle B (b-centered circle) with radius R. At the same time, the center of circle A should be a peripheral point of circles C and D, corresponding to boundary pixels c and d. If the circle drawing is repeated along the boundary pixels of circle A, pixel a will have the highest frequency of pass by the circles. In other words, pixel a
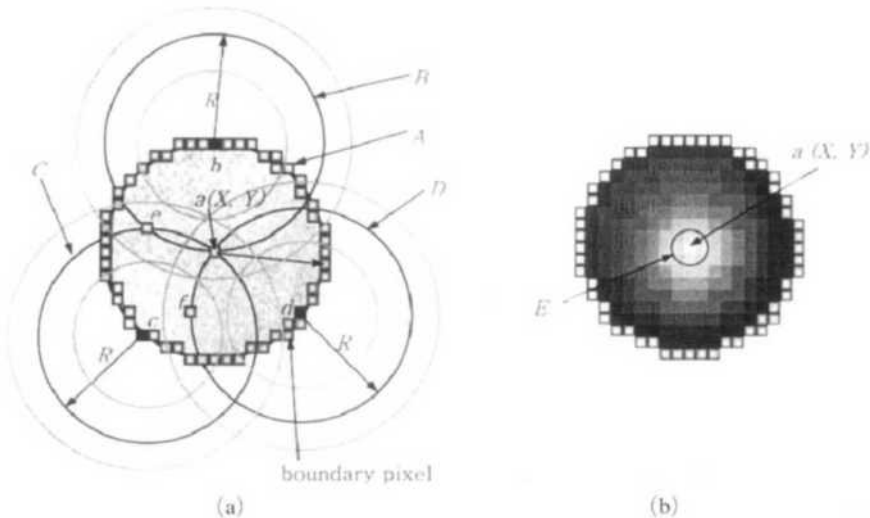

Fig. 17 Illustration of Hough transform

has the highest possibility of being the center, and it is recognized as the true center of circle A. In practice, the radius of circle A is unknown at the beginning, and the overall procedure should be repeated for various values of R. Thus, in parametric space with x-, y- and r-axes, point (X, Y, R) shows the maximum value (possibility). Figure 17(b) illustrates the possibility of being the center in the parameter space with radius R for the boundary pixels of circle A. Here, the possibility is expressed as the brightness, and the possibility viewed to be the highest at the center that corresponds to pixel $a(X, Y)$. However, the Hough transform itself is a time consuming process, and Kruis et al. (1994) proposed the sparse Hough transform to resolve this problem. In using the Hough transform to process the heavily overlapped image, the center-searching procedure has been improved by Kim and Lee (2002). Crida and de Jager (1997) used the Hough transform to perform online measurement of rock size distribution, assuming that the rock shape could be modeled using an ellipse with a reasonable accuracy. Also, due to the multi-scale nature of the rocks, multiple levels of image scale were used. However, it takes much longer to process the ellipses (compared to the circles) since there are more parameters to be considered ; hence, only one size of the rocks was detected at a particular level of the image scale to reduce the number of parameters in the parametric space.

In principle, the primary particles in the agglomerated image can be separated out and sized by examining the boundary curvature. Figure 18 shows the basic concept of this approach proposed by Kim et al.(2001). For a circle with its radius R, as shown in Fig. 18(a), the boundary curvature $(\Delta\theta/\Delta l)$ remains unchanged along the periphery l, i.e., $\Delta\theta/\Delta l = 1/R$. For an ellipse, the boundary curvature varies along the periphery with a sinusoidal shape as shown in Fig. 18(b). On the other hand, as depicted in Fig. 18(c), there are abrupt changes of the boundary curvature at the contact points of the overlapped-particle image, and this technique is very useful in handling the agglomerated particles. However, since the pixel size is not infinitesimally small, a piecewise averaging technique is needed to smooth out the saw-toothed boundary, and the details are found in the work of Kim et al.(2001).

Other than the methods of Hough transform and boundary-curvature detection, there are interesting techniques proposed by Watona and Miyanami (1995) and Kim et al. (1999) to separate the primary particles. Watona and Miyanami (1995) mentioned two methods in segregation of the overlapped granules : circle pattern matching and eight-neighbor erosion. The circle pattern matching method segregates the overlapped granules by fitting an inscribed circle, which can be used for any degree of overlapping. However, the granule shape cannot be identified with this method. The eight-neighbor erosion method transforms the level of the focused pixel to zero (background level) if any of the eight neighboring pixels have the zero level. That is, the boundary of an object image is moved inwards by one pixel. This operation can segregate the overlapped granules by repeating this step twice, at most. If segregation is not successful with this method, the image is considered as an aggregate. Once the primary granules are identified, their boundaries are moved back outward to measure the original sizes and shapes correctly. Kim et al. (1999) have proposed the convex-hull method in splitting primary particles from agglomerated

(a) Circle   (b) Ellipse   (c) Overlapped particles
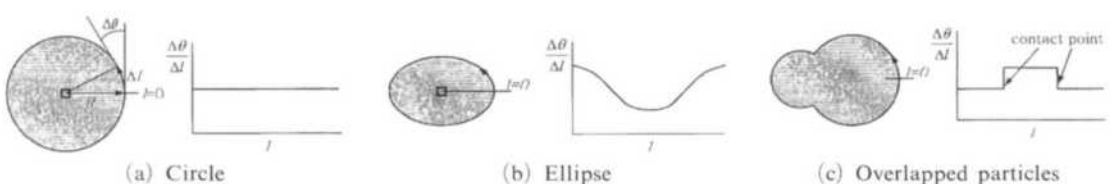
Fig. 18 Variation of boundary curvature (Kim et al., 2001)

images. For an overlapped image of two different particles, as shown in Fig. 19, the hull of the convex polygon can be determined by encompassing it with the shortest perimeter. Mostly, the distances between the adjacent pixels at the hull of the polygon appear approximately the same except for the line segments connecting two particles. The concave parts of the overlapped image exist underneath those long line segments, and the farthest boundary pixels from the segments (i.e., points a and b) are considered as the contact points of two circles. Thus, the line AB connecting points a and b is the dividing line between two particles. This technique is very useful in handling weakly overlapped images because the processing time is much shorter than the previously discussed techniques, such as the Hough transform or the boundary curvature examination. Once the primary particles are separated out, each size can be measured by finding their circumcenter as already discussed.

In order to describe the shape of the particle images, the concept of shape factor is widely adopted. The shape factor is defined as perimeter^2/area (Fantini et al., 1990) representing the deviation of the particle image from a circular shape. For a circle, this value is 4π, and if a particle is not circular this value becomes significantly greater. As a similar concept, Sudheer and Panda (2000) have used compactness, which is the reciprocal of the shape factor defined by Fantini et al. (1990). On the other hand, Lecuona et al. (2000) have used the combination of circularity and convexity. The circularity is defined as $4\pi A/P^2$, similar to the shape factor and the convexity is the ratio between the perimeter of the smallest convex hull region and the actual perimeter of the object. They considered the images having the values of circularity and convexity lower than 0.8 and 0.95, respectively, are the overlapped particles or not the ones under consideration, and those should be separated or rejected in counting. The same concept of the circularity (or shape factor) is widely adopted also in sizing bubbles or aggregates in flotation systems (Watano and Miyanami, 1995; Malysa et al., 1999; Hernandez-Aquilar et al., 2004).
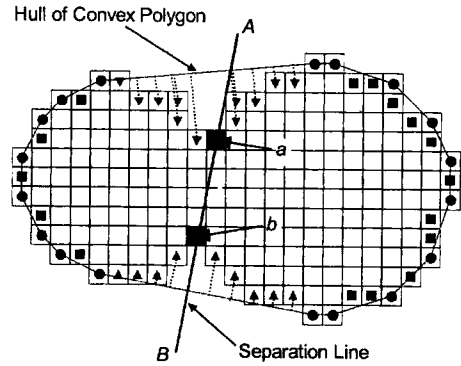

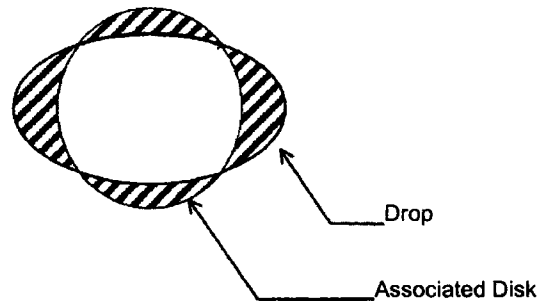**Fig. 19**   Separation of an overlapped drop image

Fig. 20   Definition of shape parameter (Malot and Blaisot, 2000)

On the other hand, Malot and Blaisot (2000) introduced the concept of the shape parameter S_p, defined as the ratio between the non-common area and the circle as shown in Fig. 20. The value of the shape parameter ranges from 0 to 2, where the value of zero corresponds to a circular 2D projection. Thus, in their work, the images of drops with large values of the shape parameter were eliminated.

5. Other Developments

Other than the in-focus criteria and the particle identification procedure discussed in the former part of this paper, some important developments related to the image processing algorithms are introduced in this section.

In order to identify particles without missing small ones, Kim and Kim (1994) divided the pattern recognition process into two major steps. The first step is to identify large particles from the entire image frame through the global threshol-

ding. Then the gray levels of the areas occupied by those already-processed large particles are replaced by the background gray-level value. In the next step, for small particles, the entire image frame is divided uniformly into subframe windows with 32×32 pixels for local thresholding. Sudheer and Panda (2000) have used the similar segmentation technique to process the photographs of sprinkler drops in flight. Later, Kim et al.(1999) improved the concept of segmentation by Kim and Kim (1994). In this case, the local processing is specific to each non-uniform-sized subframe window, which is determined by the center and the radius of each image recognized as a single particle (or object) through the global processing of the entire image frame; thereby the threshold level for each subframe can be determined differently for more accurate measurement. In other words, the concept of the local processing was proposed to reduce the measurement error by taking account of unevenness of the light illumination on the spray particles.

The concept of the two-stage process of Crida and de Jager (1997) for measurement of the rocks (solid particles) is somewhat similar to the two-step approach of Kim et al.(1999). This concept is denoted as the human visual system because the algorithm simulates the stage of preattentive vision followed by the attention focusing process, as performed by the eyes of the human beings. The purpose of the preattentive vision stage is to detect target features for further analysis in the latter stage, and the Hough transform is used assuming the particles are in elliptical shape. Then, in the attention focusing stage, target features are re-examined to determine the extent of the non-elliptical object in the image using more sophisticated process. That is, the edge points are detected (using the ellipse model) and linked to create the continuous boundary of a labeled region corresponding to the object in the image.

Another novel approach is the image processing with the laser fluorescence method. Garciamoreno (2002) analyzed images of water spray with afluorescent additive (Rhodamine B) using a pulsed laser sheet. Image frames were captured by a camera viewed perpendicular to the laser sheet. This method is capable of wide-field analysis of the instantaneous spray behavior because intensity of the light emission from each fluorescent drop is much stronger than the light intensity obtained by backward illumination. Also, the out-of-focus problem is considered relatively minor with this method because a thin laser sheet was used as the light source. This technique is extendable to the PIV method for simultaneous measurement of drop sizes and velocities in the field of interest.
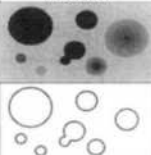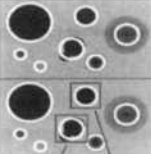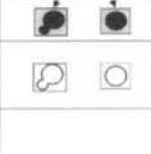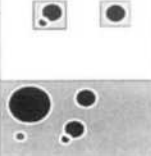
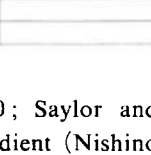Park et al.(2002) obtained SMD of gasoline sprays by using the principles of laser-induced fluorescence (LIF) and the Mie scattering of drops. For a single drop, the intensities of the LIF (I_{LIF}) and Mie (I_{Mie}) scattering signals are proportional to the cube and the square of the diameter, respectively. Thus the ratio between two intensities (I_{LIF}/I_{Mie}) obtained for a spray (a group of drops) should be proportional to SMD, and the proportionality constant could be obtained from the experiments.

6. Overall Procedure for Image Processing of Spray Particles

In the previous sections, various details on determination of the in-focus criteria and identification of spray particles have been introduced. In this section, the overall procedure of image processing utilizing those techniques is discussed. Table 1 illustrates the overall procedure to process an image frame containing spray particles based on the algorithm proposed by Kim (2000). The entire procedure consists of two major steps, namely, the global process (steps 1-2) and the local process (steps 3-9). Already explained before, this approach is advantageous because the problem of uneven brightness of image frames can be eliminated.

In the global process, first of all, a threshold level should be determined for the entire image frame. Through the boundary detection process (step 1), the original image is converted into the binary one and then the particle boundaries are sought. In this step, either the gray level (Otsu, 1979 ; Fantini et al., 1990 ; Lee et al., 1991 ; Kim,

Table 1 Overall algorithm of image processing

	Steps/Description	Illustration
	Global Process	
1	Boundary Detection in the Global Window Gray level threshold using gray level histogram Gray level gradient	
2	Circle Detection (Mass Center) Center(x, y) and Radius	
	Local Process	
3	Local Window for Each Particle	
4	Boundary Detection in Local Window Gray Level Threshold Gray Level Gradient	
5	Separation of Overlapped Particles Convex Hull, Hough Transform, Boundary Curvature Algorithm	
6	Circle Detection Circumcenter, Hough Transform, Boundary Curvature Algorithm	
7	Out-of-Focus Particle Rejection Gray Level Gradient (GI), Value of Contrast (VC) Combination of GI and VC	
8	Depth-of-field Correction	
9	Calculation of Mean Diameter	

2000 ; Sudheer and Panda, 2000 ; Saylor and Jones, 2002) or the gray-level gradient (Nishino et al., 2000 ; Kim and Lee, 2002) of the particle image may be used as the threshold criterion. In the next step, the approximate radii and the locations of the particles or 'particle-like' objects (such as the overlapped particles and the odd-shaped materials) are identified by searching the their centers using Eqs. (11) and (12).

In the second stage, the local process starts with step 3, dividing the entire image frame into local windows each covering a single particle or a 'particle-like' object. Then, in step 4, the boundary of the object in each local window is sought. Similar to step 1 of the global process, either the gray-level threshold (Kim and Kim, 1994 ; Lebrun et al., 1996 ; Kim et al., 1999 ; Kim, 2000 ; Malot and Blaisot, 2000 ; Koh et al., 2001) or the gray-level gradient threshold (Nishino et al., 2000 ; Kim and Lee, 2002) may be used. Once the object boundaries are detected, primary particles are separated out from the overlapped images (Kruis et al., 1994 ; Kim et al.,

1999 ; Kim et al., 2001 ; Kim and Lee, 2002) and the odd-shaped materials are filtered out (Kim and Lee, 1990), if there are any, as in steps 5 and 6. In the next step (step 7), the out-of-focus particles, which have ambiguous boundaries, are eliminated using the in-focus criteria (Fantini et al., 1990 ; Kim and Kim, 1994 ; Lebrun et al., 1996 ; Lecuona et al., 2000 ; Malot and Blaisot, 2000 ; Koh et al., 2001). Then, in step 8, the depth-of-field correction (Koh et al., 2001) is performed to take account of different field depths of each size-group contained in a fixed measuring volume. Finally (step 9), the particles recognized as the correct ones in the image frame are counted and sized for analysis.

7. Conclusions and Suggestions

In this article, recent development of the image processing technique to count and size particles is introduced, which is essentially important in the field of spray/atomization technology. Basically, there are two main issues to be resolved. One is the out-of-focus problem and another is the method of particle identification from the focused images.

The out-of-focus particles are the largest error sources in counting and sizing them in a measuring volume. Therefore most of the works were concentrated on the establishment of the in-focus criteria. The gray level gradient and the value of contrast were introduced as the indicators of the degree of focus. Each indicator is suitable to different size ranges : the gray level gradient for large particles and the value of contrast for small particles. To cover those size ranges simultaneously, a unified in-focus criterion has been proposed.

Pattern recognition and size measurement are the main subjects of the particle identification. In most cases, particle diameters can be obtained from the projected area of the particles. To process the partially detected or overlapped particles, the convex-hull method, Hough transform, pattern matching through Fourier transform, and the boundary-curvature detection method have been developed. To represent the non-circularity

of the particle images, various shape factors were introduced.

Improvement of the image processing technique was always possible with the rapid progress in computing hardware. Most of the basic concepts regarding the image processing of the spray drops/particles are established so far. However, there are several important problems still to be resolved. Handling of non-spherical particles is one of them since there are various shapes other than spheres (circles) or ovals (ellipses). Systematic classification of the particle shape should be performed prior to process them. Another is the dependency of the measured results on the system hardware. Determination of the in-focus criteria and the threshold levels depends strongly on the optical arrangement (i.e., optical parameters, such as focal length, aperture size, etc.). Hence, especially for real-time measurement of spray drops, there should be a general (or a standard) procedure to match the optical parameters and the image-processing algorithm to get consistent results. Finally, considering that the ultimate goal of the image processing technique is to recognize the objects as the human vision, introduction of the concepts of the artificial intelligence and the neural network may be another break through in this field.

Acknowledgment

References

Chigier, N., 1983, "Drop Size and Velocity Instrumentation," Prog. Energy Combust. Sci., Vol. 9, pp. 155~177.

Chigier, N., 1991, "Optical Imaging of Sprays," Prog. Energy Combustion Sci., No. 17, pp. 211~262.

Crida, R. C. and de Jager, G., 1997, "An Approach to Rock Size Measurement based on a Model of the Human Visual System," *Minerals Engineering*, Vol. 10, No. 10, pp. 1085~1093.

Cruvinel, P. E., Vieira, S. R., Crestana, S., Minatel, E. R., Mucheroni, M. L. and Neto, A. T., 1999, "Image Processing in Automated Measurements of Raindrop Size and Distribution," *Computers and Electronics in Agriculture*, Vol. 23, pp. 205~217.

Fantini, E., Tognotti, L. and Tonazzini, A., 1990, "Drop Size Distribution in Sprays by Image Processing," *Computers chem. Engng.*, Vol. 14, No. 11, pp. 1201~1211.

Garciamoreno, C. J., 2002, "Heat Transfer in Two-Phase Stagnation Point Flow," M. S. Thesis, The University of Michigan, USA.

Gonzalez, R. C. and Woods, R. E., 1993, Digital Image Processing, Addison Wesley.

Hernandez-Aquilar, J. R., Coleman, R. G., Gomez, C. O. and Finch, J. A., 2004, "A Comparison between Capillary and Image Techniques for Sizing Bubbles in Flotation Systems," *Mineral Engineering*, Vol. 17, pp. 53~61.

Kim, J. Y., 2000, "Study of Internal Flow Characteristics and Atomization Performance of Effervescent Atomizers," Ph. D Thesis, KAIST, Korea.

Kim, J. Y., Chu, J. H. and Lee, S. Y., 1999, "Improvement of Pattern Recognition Algorithm for Drop Size Measurement," *Atomization and Sprays*, Vol. 9, No. 3, pp. 313~329.

Kim, K. S. and Kim, S. S., 1994, "Drop Sizing and Depth-of-Field Correction in TV Imaging," *Atomization and Sprays*, Vol. 4, pp. 65-78.

Kim, I. G. and Lee, S. Y., 1990, "A Simple Technique for Sizing and Counting of Spray Drops Using Digital Image Processing," *Exp. Thermal Fluid Sci.*, Vol. 3, pp. 214~221.

Kim, Y. D. and Lee, S. Y., 2002, "Application of Hough Transform to Image Processing of Heavily Overlapped Particles with Spherical Shapes," *Atomization and Sprays*, Vol. 12, No. 4, pp. 451~461.

Kim, Y. D., Lee, S. Y. and Chu, J. H., 2001,

"Separation of Overlapped Particles Using Boundary Curvature Information," Proceedings of the 6th Annual Conference on Liquid Atomization and Spray Systems (ILASS-Asia 2001), pp. 259~264.

Koh, K. U., Kim, J. Y. and Lee, S. Y., 2001, "Determination of In-focus Criteria and Depth of Field in Image Processing of Spray Particles," *Atomization and Sprays*, Vol. 11, No. 4, pp. 317~333.

Kruis, F. E., Denderen, J. V., Burrman, H. and Scarlett, B., 1994, "Characterization of Agglomerated and Aggregated Aerosol Particles Using Image Analysis," *Part. Part. Syst. Charact.*, Vol. 11, pp. 426~435.

Lebrun, D., Touil, C. E. and Ozkul, C., 1996, "Methods for the Deconvolution of Defocused-Image Pairs Recorded Separately on Two CCD Cameras : Application to Particle Sizing," *Applied Optics*, Vol. 35, No. 32, pp. 6375~6381.

Lecuona, A., Sosa, P. A., Rodriguez, P. A. and Zequeira, R. I., 2000, "Volumetric Characterization of Dispersed Two-phase Flows by Digital Image Analysis," *Measurement Science and Technology*, No. 11, pp. 1152~1161.

Lee, S. Y., Park, B. S. and Kim, I. G., 1991, "Gray Level Factors Used in Image Processing of Two-Dimensional Drop Images," *Atomization and Sprays*, Vol. 1, No. 4, pp. 389~400.

Malot, H. and Blaisot, J. B., 2000, "Droplet Size Distribution and Sphericity Measurements of Low-Density Sprays through Image Analysis," *Part. Part. Syst. Charact.*, No. 17, pp. 146~158.

Malysa, K., Ng, S., Cymbalisty, L., Czarnecki, J. and Masliyah, J., 1999, "A Method of Visualization and Characterization of Aggregate Flow inside a Separation Vessel, Part 1. Size, Shape and Rise Velocity of the Aggregates," *Int. J. Mineral Processing*, Vol. 55, pp. 171~188.

Nishino, K., Kato, H. and Torii, K., 2000, "Stereo Imaging for Simultaneous Measurement of Size and Velocity of Particles in Dispersed Two-Phase Flow," *Measurement Science and Technology*, No. 11, pp. 633~645.

Oberdier, L. M., 1984, "An Instrumentation System to Automate the Analysis of Fuel-Spray Images using Computer Vision," *ASTM*, No.

848, pp. 123~136.

Otsu, N., 1979, "A Threshold Selection Method from Gray Level Histogram," *IEEE Transactions on Systems, Man and Cybernetics*, Vol. SMC-9, No. 1, pp. 62~66.

Park, S., Cho, H., Yoon, I. and Min, K., 2002, "Measurement of Droplet Size Distribution of Gasoline Direct Injection Spray by Droplet Generator and Planar Image Technique," *Measurement Science and Technology*, Vol. 13, pp. 859~864.

Ramshaw, C., 1968, "A Technique for Drop Size Measurements by Direct Photography and Electronic Image Size Analysis," *J. Inst. Fuel*, No. 41, 288~292.

Saylor, J. R. and Jones, B. K., 2002, "A Method for Increasing Depth of Field during Droplet Imaging," *Review of Scientific Instruments*, Vol. 73, No. 6, pp. 2422~2427.

Shen, L., Song, X., Murai, Y., Iguchi, M. and Yamamoto, F., 2001, "Velocity and Size Measurement of Falling Particles with Fuzzy PTV," *Flow Measurement and Instrumentation*, Vol. 12, pp. 191~199.

Sudheer, K. P. and Panda, R. K., 2000, "Digital Image Processing for Determining Drop Sizes from Irrigation Spray Nozzles," *Agricultural Water Management*, No. 45, pp. 159-167.

Swithenbank, J., Beer, J., Taylor, D. S., Abbot, D. and McGreath, G. C., 1977, "A Laser Diagnostic Technique for the Measurement of Droplet and Particle Size Distributions," *Prog. Aeronaut. Astronaut.*, Vol. 53, pp. 421~427.

Watano, S. and Miyanami, K., 1995, "Image Processing for On-line Monitoring of Granule Size Distribution and Shape in Fludized Bed Granulation," *Powder Technology*, Vol. 83, pp. 55~60.

Wild, P. N. and Swithenbank, J., 1986, "Beam Stop and Vignetting Effects in Particle Size Measurements by Laser Diffraction," *Applied Optics*, No. 25, pp. 3520~3526.

Zhang, G. J. and Ishii, M., 1995, "Isokinetic Sampling Probe and Image Processing System for Droplet Size Measurement in Two-Phase Flow," *Int. J. Heat Mass Transfer*, Vol. 38, No. 11, pp. 2019~2027.